10-6-2014

Interseismic Locking on the Hikurangi Subduction Zone: Uncertainties from Slow-Slip Events

Robert McCaffrey
Portland State University

Citation Details

Mccaffrey, R. (2014), Interseismic locking on the Hikurangi subduction zone: Uncertainties from slow-slip events, J. Geophys. Res. Solid Earth, 119, 7874-7888

AGU PUBLICATIONS

JGR

Journal of Geophysical Research: Solid Earth

RESEARCH ARTICLE
10.1002/2014JB010945

Key Points:
- Modern locking on the Hikurangi subduction zone is reevaluated
- Transient events produce large uncertainties in GPS velocities
- Decade-scale locking patterns may not hold in regions of slow slip

Supporting Information:
- Readme
- Table S1
- Table S2
- Table S3
- Table S4
- Figure S1
- Figure S2
- Figure S3
- Figure S4

Correspondence to:
R. McCaffrey,
r.mccaffrey@pdx.edu

Citation:
McCaffrey, R. (2014), Interseismic locking on the Hikurangi subduction zone: Uncertainties from slow-slip events, *J. Geophys. Res. Solid Earth*, *119*, 7874–7888, doi:10.1002/2014JB010945.

Received 8 JAN 2014
Accepted 27 AUG 2014
Accepted article online 2 SEP 2014
Published online 6 OCT 2014

Interseismic locking on the Hikurangi subduction zone: Uncertainties from slow-slip events

Robert McCaffrey[1]

[1]Department of Geology, Portland State University, Portland, Oregon, USA

Abstract Interseismic locking on the Hikurangi subduction zone in New Zealand is examined in light of alternative assumed locking distributions and the impact of transients (slow-slip and volcanic sources) on temporal and spatial resolution. The modern pattern of locking in the north is poorly resolved and, based on simulations of possible transient behavior, may be an ephemeral feature of the subduction cycle. While there appears to be some contemporary locking in the northern half of the Hikurangi subduction zone (HSZ), its location is model dependent, and hence, its relationship to structure, slow-slip, or any transition zone there is unclear. Simulations of site velocities using the 14 year history of transient events reveal that in the timescale of the interseismic period the northern half of the HSZ could be either locked or unlocked, and this may not be resolvable for decades. In the southern half, there is strong contemporary locking in the 15 to 40 km depth range, but again, the slow-slip history leads to uncertainty in the long-term pattern. Slow-slip events not only reduce the long-term locking by aseismic slip but also greatly hinder our ability to see it. It is within the range of possible models that the slip deficit rate at the HSZ is more uniform along strike, and the modern appearance is controlled by the particular pattern of transients over the past 10 to 20 years when the GPS data were collected. Similarly, uncertainties in surface velocities will be large at any subduction zone with large transients.

1. Introduction

Modern locking on subduction faults inferred from geodetic data is one possible method of estimating the potential slip of future large earthquakes and for understanding the role of subduction zone structure in controlling seismic slip. The agreement of the preseismic locking pattern at the Japan Trench [*Loveless and Meade*, 2010] with the 2011 Tohoku-oki slip pattern [*Simons et al.*, 2011] provide some support for the predictive capabilities of geodetic data.

Interseismic locking models, that is, those thought to represent the steady loading during the seismic cycle and possibly indicating where seismic slip might eventually occur, are generally derived from GPS data that are assumed to have been collected over a long enough period that short-term deviations from linearity in the time series have evened out. For example, in Cascadia, 80 years of leveling data [*Burgette et al.*, 2009] and 20 years of GPS observations [*McCaffrey et al.*, 2013] provide a view of the deformation that averages out the small, frequent (~yearly) slow-slip events. These data allow a view of the locking over a relatively long portion of the earthquake recurrence interval, thought to be ~500 years [*Goldfinger et al.*, 2012]. For most subduction zones, the geodetic observation period is shorter and it is not clear how the contemporary locking relates to the longer period (i.e., a large fraction of the seismic cycle). For subduction zones with large transient components, the modern locking pattern is a snapshot of a time-varying process and may or may not resemble the average interseismic locking.

In the presence of slow-slip events (SSEs) and other transients in GPS time series, three slopes are of interest (Figure 1). The intertransient rate (slope of the blue line) represents the loading of the crust in the time between transients, as well as steady motions due to block motions and crustal strain (e.g., faulting). It seems to be stable through time in New Zealand, Cascadia, and elsewhere. Part of this loading is released in SSE, and part may be stored for an earthquake. The part that remains after the SSE, or the interseismic rate (Figure 1; slope of the purple line), reveals long-term loading of the crust and includes the component of elastic strain building to the next earthquake. A third slope (red line) is the slope of the geodetic time series from which we infer the other two rates. If we use an appropriate noise model, the slope of the time series (red line) and its uncertainty should provide an estimate of the interseismic rate.

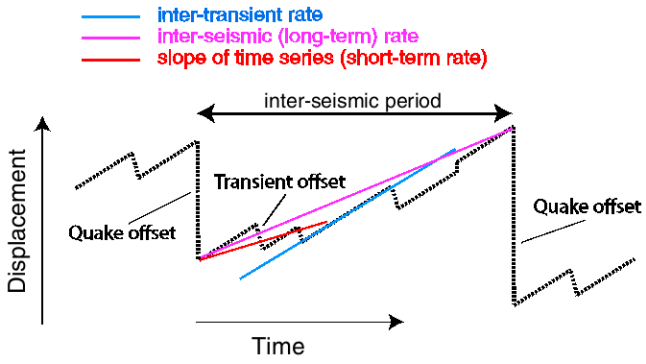

Figure 1. Definition of intertransient and interseismic velocities and the slope of the time series in the presence of transient offsets. Dotted line represents GPS position time series.

Because the interseismic rate is the intertransient rate corrected for the transient offsets, its accuracy depends on knowing the temporal behavior of transients. In the case of GPS time series observed at subduction zones with large site displacements due to slow-slip or other transient events, knowledge of the short SSE history may not be sufficient to understand its long-term behavior. This problem is entirely analogous to that of understanding earthquake behavior through many cycles gleaned from a short seismic history. One goal of this paper is to examine how important is the effect of slow slip on the estimated GPS-derived rates and long-term locking patterns inferred from them for the Hikurangi subduction zone of New Zealand. The results are also applicable to other subduction zones with large SSE.

The Hikurangi subduction zone (HSZ) off the east coast of the North Island, New Zealand, accommodates westward subduction of the Pacific plate relative to Australia at about 40 to 50 mm/yr (Figure 2). Because the subduction zone is curved and oblique to the relative convergence direction, the trench-normal subduction rate decreases to the south and eventually relative motion becomes largely shear in the northern part of South Island. Due to the slip partitioning driven by the oblique convergence and active spreading in the Taupo Volcanic Zone (TVZ; Figure 2), the upper plate has fragmented, producing several crustal faults and rapidly rotating blocks [*Walcott*, 1984; *Wallace et al*., 2004]. Because the coastal blocks accommodate slip partitioning, the convergence of the Pacific with the eastern North Island coastal region is nearly orthogonal to the margin (Figure 2; red vectors) but west of the North Island's axial deformation zone (Wellington Fault; Figure 2), relative motion on the HSZ is highly oblique again.

Locking on the HSZ has been estimated by *Wallace et al*. [2004, 2012] using elastic half-space dislocation models constrained by 10 to 20 years of GPS-derived surface horizontal velocities. These models show a very sharp gradient between low-level, shallow locking in the north and stronger and deeper locking in the south. This pattern has since been compared to more permanent properties of the subduction zone, such as attenuation patterns, electrical conductivity, pore pressure, and so on [for example, *Eberhart-Phillips and Reyners*, 2012; *Heise et al*., 2013]. The assumption by those authors is that the 10 to 20 year locking pattern has the same level of permanency as the other properties.

The initial locking model, from *Wallace et al*. [2004], was constrained by horizontal survey-mode GPS velocities from 1991 to 2003 (here obtained from J. Beavan; the velocities are in two fields, called NI2003 field from the North Island and SI2003 field from the northern 200 km of the South Island). An update presented by *Wallace et al*. [2012] included additional survey-mode observations (2006 and 2008) from the southern part of the North Island and continuous mode GPS (cGPS) that started about the year 2000. The velocity fields used by *Wallace et al*. [2012] were not made available for this study. However, the GeoNet cGPS data, which are publicly available (ftp.geonet.org.nz), are dense in the region of the newer survey data. In this paper, I combine the velocities from NI2003 and SI2003 with those estimated from the cGPS from 2000 through May 2014. In the initial analyses of the cGPS data, I use the uncertainties estimated by standard GPS processing techniques that assume the time series are linear and affected by stationary, power law noise [*Hackl et al*., 2011; *Williams*, 2003a, 2003b]. After that, I estimate uncertainties in the site velocities that are expected in the presence of slow-slip events (a nonstationary process) and investigate their impact on the long-term locking models.

2. Update of Locking Model

Using the combined NI2003, SI2003, and cGPS velocity fields, I run inversions to estimate locking on the HSZ using three assumed parameterizations (Figure 3). Locking here is defined kinematically as ϕV where ϕ is the

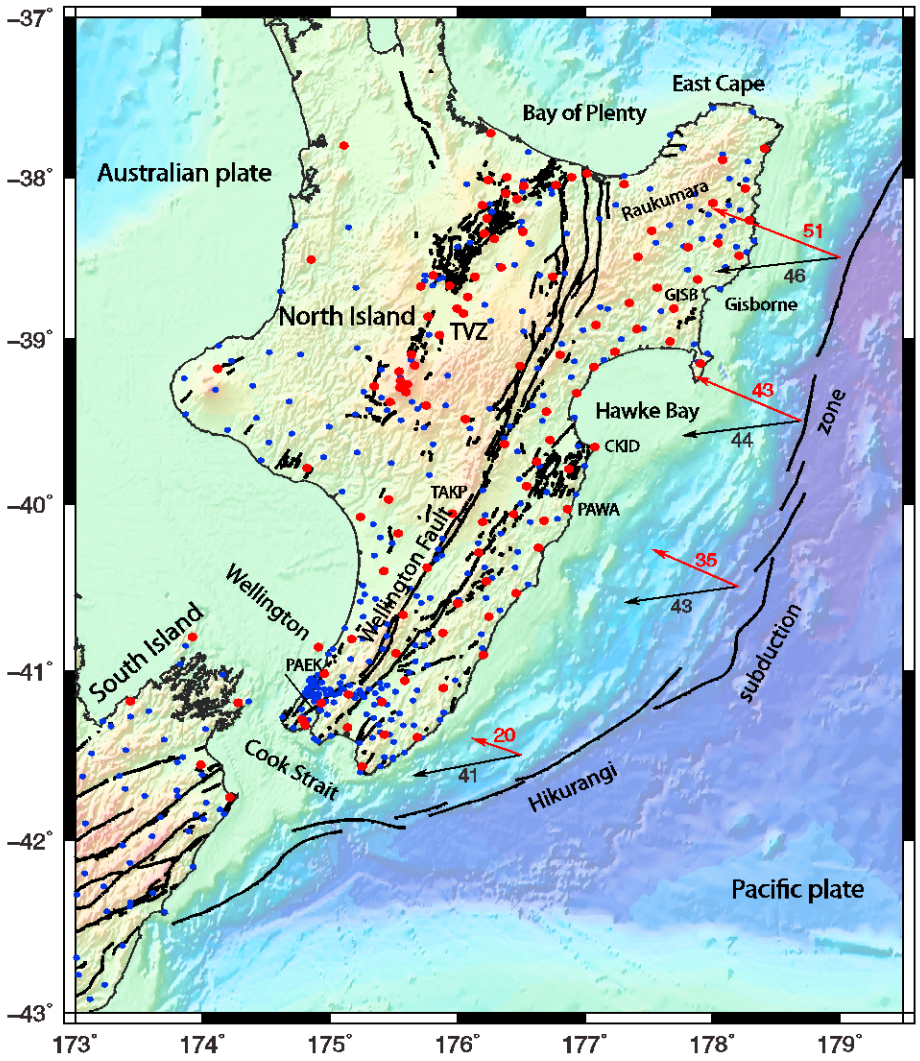

Figure 2. Location map of the North Island, New Zealand, and the Hikurangi subduction zone. Black arrows show motion of the Pacific plate relative to Australian plate, and red are Pacific relative to coastal blocks (rates in mm/yr). Red dots are continuous GPS sites of GeoNet, and blue are survey-mode sites. TVZ = Taupo Volcanic Zone. Site codes are shown for cGPS sites discussed in the text.

part of the relative plate motion across the faults that is stuck, or one minus the creeping fraction, and V is the relative velocity across the fault derived from relative plate (block) motions (ϕV is also called the slip rate deficit with units of mm/yr). Estimated in this way from surface GPS velocities and an elastic model of the Earth, locking represents a rate of stress increase on the fault. The first locking parameterization used (called the Exponential model), similar to that used by *Wallace et al*. [2004, 2012], proposed by *Wang et al*. [2003], and modified by *McCaffrey et al*. [2007], holds that $\phi = 1$ (full locking) from the deformation front to a depth Z_1, and decreases by an exponential function to become zero at depth Z_2 and below. The decay across the transition zone (between Z_1 and Z_2) is controlled by the shape parameter γ (see equation (3) of *McCaffrey et al*. [2007]). This parameterization assumes the locking is greatest at the trench and decreases monotonically with depth. In the second assumed distribution, the Gaussian model, locking is a Gaussian function of depth where the mean depth, the spread in depth, and the peak ϕ are all estimated. The third method divides the fault surface into a grid of finite regions of approximately 40 × 40 km and solves for uniform ϕ at each of them. For all models the crustal fault geometry is similar to that of *Wallace et al*. [2012], and free parameters include block rotations, locking on crustal faults and uniform strain rates in two blocks that comprise the TVZ. The models all have 1044 observations and 142 free parameters (9 to rotate 3 velocity fields into the Australia reference frame, 75 for HSZ locking, 16 for crustal fault locking, and the rest for block kinematics).

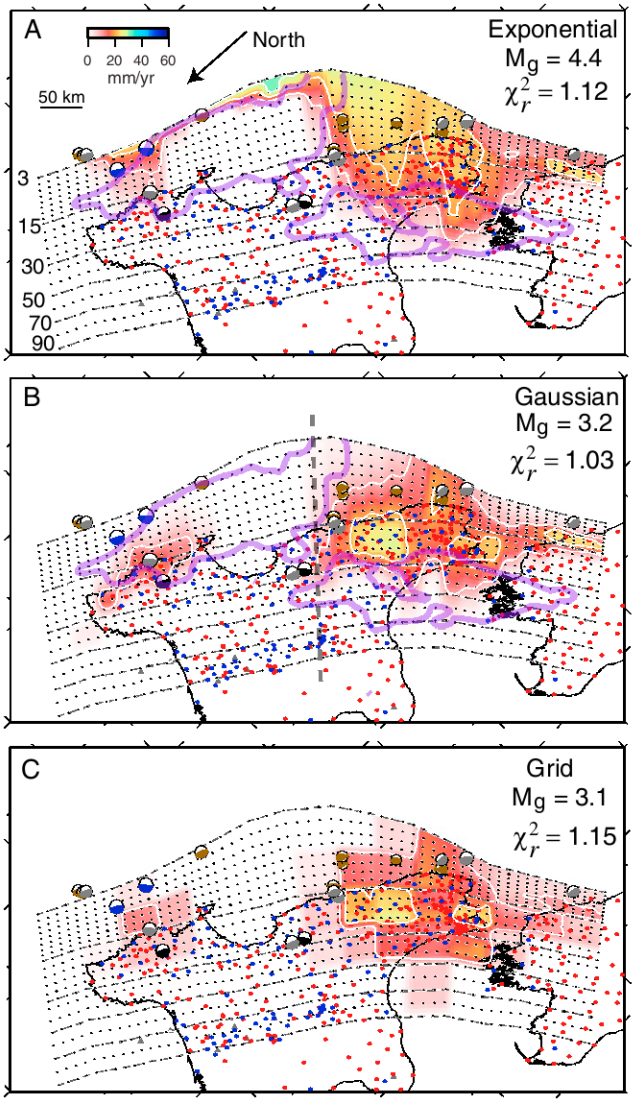

Figure 3. Locking models based on combined NI2003, SI2003, and cGPS velocity fields (covering ~20 years). (a) Assumes an exponential decay in locking with depth, (b) uses a Gaussian change in locking with depth, and (c) uses a grid. The reduced chi-square data misfit is χ_r^2, and M_g is the geodetic moment rate of the locking in 10^{19} N m/yr. Dashed lines are contours of the plate interface, labeled in kilometers at their northern ends in Figure 3a; small black dots are nodes in the plate interface. Red dots are survey-mode GPS site locations, and blue are cGPS. Colored shading shows the slip rate deficit in mm/yr contoured at 10 mm/yr. Black beach balls are from probable plate interface earthquakes with well-controlled depths [*Webb and Anderson*, 1998, their events B and U]; gray are global centroid moment tensor solutions [*Ekström et al.*, 2012], brown from GeoNet, and blue are the tsunamigenic events of 1947 [*Doser and Webb*, 2003]. All mechanisms except GeoNet are plotted at their International Seismological Centre epicenters [*International Seismological Centre*, 2011]. Purple curves outline the extent of cumulative slow slip for 2000–2014 (the 100 mm contour).

The cGPS velocities were estimated from GeoNet time series (ftp.geonet.org.nz/solutions/regional-filtered) for 2000 through May 2014. Not all sites have been operating since 2000 as the network has grown through time. For each component of each time series a linear regression was performed to estimate the slope, i.e., a velocity uncorrected for transients. The online GeoNet time series do not include position uncertainties so I assumed 2.0 mm for east and north and 5.0 mm for the vertical. The uncertainties in velocities were estimated with an error model that includes both white noise and colored noise [*Williams*, 2003a; *Hackl et al.*, 2011] using the Python code of M. Hackl. For example, this procedure resulted in uncertainties of 0.19 and 0.11 mm/yr for east and north and 0.30 mm/yr vertical at site AUCK which is far from both the deforming zone and slow-slip events (SSEs) and has a 14 year duration. At the coastal site GISB with a 12 year record and SSE offsets up to ~30 mm, the uncertainties were 2.25, 1.09, and 0.85 mm/yr for the east, north, and vertical, respectively. These uncertainties at GISB are larger than typical for a site of similar duration since they account in part for scatter due to the transients (largely represented by random walk in the *Hackl et al.* [2011] method). All velocities and their uncertainties are given in the supporting information. The survey-mode velocity uncertainties, as described in *Wallace et al.* [2004], were estimated with a white noise component and using a scaling factor to account for colored noise. In the inversions the velocity fields' uncertainties are scaled to make the sum of weights of the cGPS field approximately equal to the sum of the weights of the two survey-mode fields and to bring the normalized RMS of the misfits close to unity (scale factors were 1.5 for cGPS, 2.0 for NI2003, and 2.5 for SI2003).

The inversions are performed with tdefnode [*McCaffrey*, 2009]. The slab geometry is digitized from *Ansell and Bannister* [1996], as in earlier studies, and is sampled along 61 margin-normal vertical profiles at 21 depths, forming an irregular grid of nodes that follow the three-dimensional shape of the slab surface. For the first two types of models, locking is defined by the three parameters for the functions described above along

profiles extending down the dip of the slab. In the inversions the profiles are grouped into 25 separate segments; within each segment the locking function parameters are kept the same but allowed to vary between segments. For the Grid model, the locking is estimated at 75 patches formed by groups of 4 × 4 nodes (approximately 40 × 40 km). Smoothing of the locking is applied by imposing a penalty on its second derivative (curvature), and excess (unnecessary) locking is damped by imposing a penalty on the sum of the locking fractions (to reduce any locking that does not produce a compensating improvement to the data fit). In the inversion, parameters are adjusted to minimize the following sum:

$$\mathbf{R}^T\mathbf{W}\mathbf{R} + \alpha\sum_{i=1,N}\left(\frac{d^2\phi_i}{dx^2}\right)^2 + \beta\sum_{i=1,N}\left(\frac{d^2\phi_i}{dw^2}\right)^2 + \lambda\sum_{i=1,N}\left(\frac{\phi_i}{N}\right) + \sum\mathbf{P}_k \quad (1)$$

where **R** is the data residual vector; **W** is the weight matrix; α, β, and λ are scaling factors for damping; ϕ is the locking fraction (value between 0 and 1); x and w are the along-strike and downdip directions; N is the number of nodes; and $\mathbf{P}_k$ represents other penalties. The first term is the χ^2 data misfit, the second and third are along-strike and downdip smoothing, and the fourth damps the total slip rate deficit. The impact of the damping on the normalized residuals (NRMS) is evaluated with a suite of inversions using the Exponential and Gaussian parameterizations and a range of the damping factor α from 10^1 to 10^7 (with $\beta = 0$, $\lambda = 2.0$; Figure S1 in the supporting information). For low damping, α up to about 10^4, there is little change in NRMS, indicating that the data have some level of inherent spatial smoothness. Above $\alpha = 10^6$ the fit degrades, suggesting the model is oversmoothed. The results with damping factor of $\alpha = 10^5$ are shown in Figure 3 while some of the other models are shown in the supporting information (Figure S2). The Exponential models consistently have about a 10% poorer fit than the Gaussian models (Figure S1). A series of checkerboard tests to examine resolution of the current data for locking on the HSZ (Figure S3) show that locking within ~50 km of the deformation front cannot be resolved except in the south where the coast is closer to the trench. Deeper parts of the HSZ are also not as well resolved. Beneath the North Island, where data are available, features at about 40 km wavelength seem to be resolved (Figure S3).

The best fit locking models are shown in Figure 3 in terms of their slip rate deficits (locking fraction times the relative fault slip rate). The model in Figure 3a used a similar parameterization as *Wallace et al*. [2004, 2012] and gives a similar looking result. Along the north coast, the slip rate deficit (SRD) is less than ~10 mm/yr (< ~20% locked). This particular parameterization places most locking in the north well offshore near the deformation front where it is least resolved. The Gaussian (Figure 3b) and Grid (Figure 3c) models both show locking beneath land (> 15 km depth) in the north. The Gaussian model provides a ~8% improvement in fit to the data (same smoothing applied). *Wallace and Beavan* [2010] suggested that the SSE in the north, which are largely offshore, occur at the downdip edge of locking based on a model like Figure 3a (purple lines in Figure 3 are 100 mm contour of cumulative slow slip for 2000–2014). This pattern holds with the Exponential model (Figure 3a). However, the alternative models in Figures 3b and 3c place the north coast locking along the downdip edge (west) of the SSE. In the central section of the HSZ there are both shallow and deep SSEs, with a locked patch between them (Figure 3b). *Webb and Anderson* [1998] modeled the waveforms of two *M*5.6 earthquakes and found well-constrained depths of 24 and 26 km (black beach balls in Figure 3). These are both well downdip of the inferred locking in Figure 3a but on the edge of locked patches in the Gaussian model (Figure 3b). They are also downdip of the shallow slow-slip events in the north and central HSZ (Figure 3b). The southern event is curiously in the small gap between the shallow and deep SSE contours.

In the south, the models are similar except that offshore locking is greatly reduced in the Gaussian and Grid models. Offshore locking is poorly resolved and not required by the data. Where the subduction front is close to the coast, the data are sensitive to shallow locking, but still not out to the deformation front (Figure S3). The downdip edge of the locking pattern is similar among the models and coincides with the SSE.

3. Effects of Transients on Locking Estimates

3.1. Estimates of SSE Offsets

The foregoing locking models are based on ~20 years of GPS observations and strictly speaking represent the time-averaged locking during that time period only. Nevertheless, as noted earlier, many authors have related a HSZ locking pattern similar to Figure 3a to structural and geophysical properties of the subduction zone that are much longer lived. In doing so, it is implied that the 20 year locking pattern is more or less

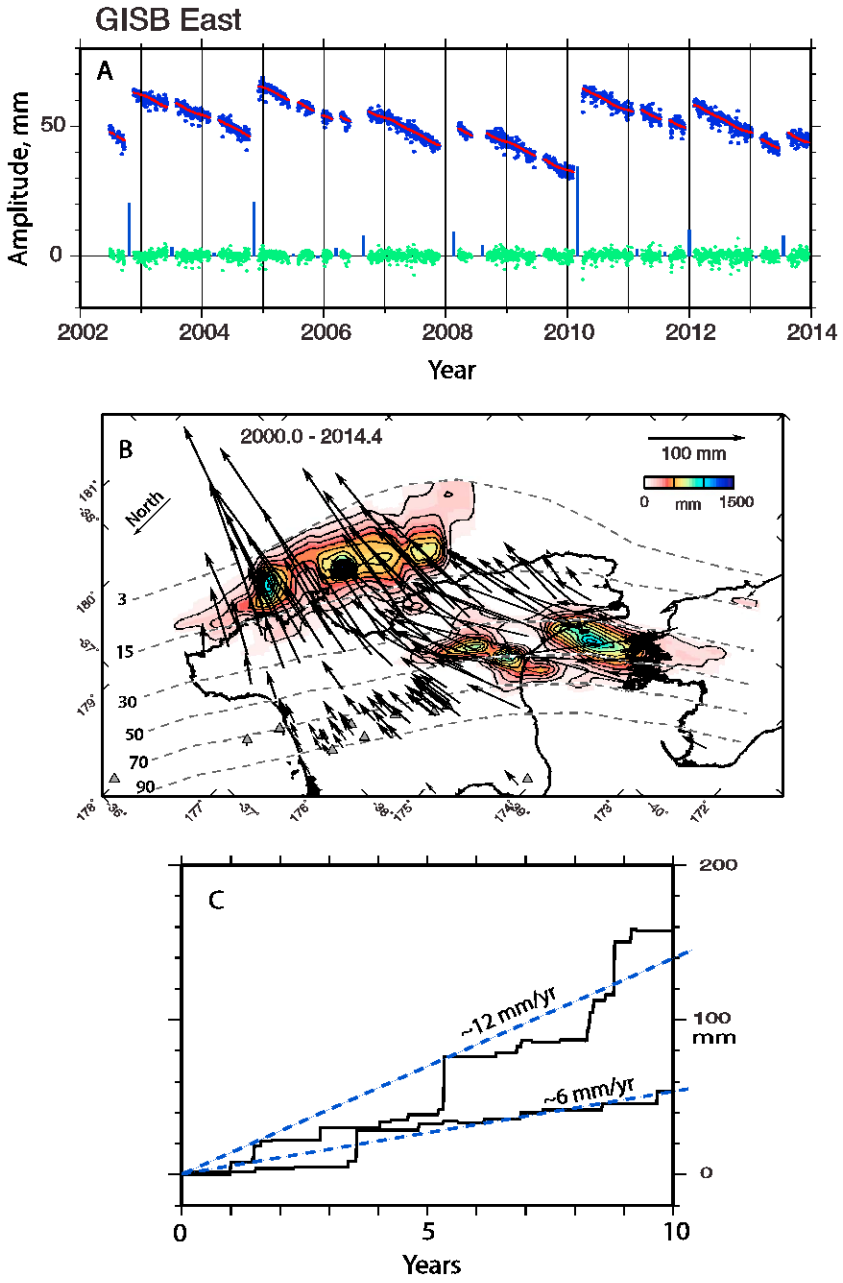

Figure 4. (a) GISB GPS east time series (blue dots), predicted time series (red), residual time series after removal of slope, offsets and seasonal signal (green), and estimated SSE and earthquake offsets (blue lines). The time series has been detrended. (b) Cumulative slow slip (in 100 mm contours) on the HSZ and total site displacements. (c) Examples of two time series scenarios generated by a random occurrence of transient events for the east component of site GISB. Slopes of dashed lines are approximate velocities due to the transient offsets.

permanent. Is there justification to thinking that the locking is long lived? Here I examine that question in the context of the transient behavior of the HSZ.

The Hikurangi subduction zone has produced more than 30 slow-slip events over the past 14 years [*Douglas et al*., 2005; *Wallace and Beavan*, 2010; *McCaffrey*, 2013]. Some have produced displacements at GPS sites of more than 3 cm. I suggest that they can have a profound impact on the estimated interseismic GPS site velocities and hence on our estimates of locking. In this section I estimate the velocity variations that can arise from the random timing and sizes of the slow-slip events and how these might influence locking estimates.

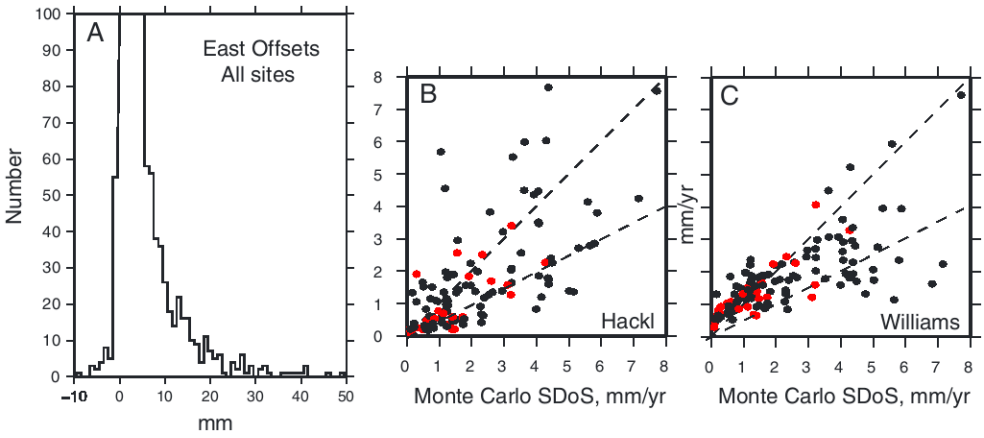

Figure 5. (a) Cumulative histogram of east offsets at all cGPS sites for all SSE from 2000 to 2014. (b) Comparison of east rate standard deviations of slopes (SDoSs) estimated with Monte Carlo versus rate uncertainties using the *Hackl et al.* [2011] method. Dashed lines are at slopes of 1 and ½. Red dots are for sites with more than 10 years duration. (c) Same as Figure 5b comparing Monte Carlo to uncertainties using the *Williams* [2003b] method.

Offsets due to slow-slip events, volcanic movements, earthquakes, and afterslip are estimated from an inversion of GeoNet time series from 2000 through May 2014 [*McCaffrey*, 2013] using the method outlined in *McCaffrey* [2009] (all estimated offsets are listed in Table S4). Figure 4a shows the east component of the site GISB time series and its estimated offsets. This time series has an 11.5 year average rate close to zero (−0.9 mm/yr), while the intertransient velocity is −11.3 mm/yr. The difference of more than 10 mm/yr highlights the large effect that slow-slip events have on the site's motion. The modeling of the transient events also allows predictions of offsets at cGPS sites that were not running at the time of the transient (offsets and subsequent uncertainties could also be estimated for the survey-mode sites, for example, but I use only the cGPS sites here). The total slip in SSE and the total site displacements estimated from the time series are shown in Figure 4b.

For the locking models discussed above, the uncertainties in the cGPS velocities were estimated using the *Hackl et al.* [2011] method that treats the noise as a power law distribution. *Williams* [2003b] examined the effect of offsets in GPS time series on the rate uncertainties. He suggested that the rate uncertainty σ_ρ can be estimated by a random walk process; $\sigma_\rho^2 = p\,\sigma_d^2/T$ where p is the per day event probability, σ_d^2 is the variance of the detrended time series, and T is the duration of the time series in days. In this method, the offsets are assumed to follow a Gaussian distribution with a mean of zero. However, the offsets from SSE in New Zealand have a non-Gaussian, skewed distribution with most being positive (eastward) (Figure 5a). To explore the impact of SSE offsets, in the next section I use a Monte Carlo approach to estimate rate uncertainties using the observed distribution of offsets at the sites and compare them to the Hackl and Williams estimates.

3.2. Monte Carlo Simulation of Time Series

The goal of using GPS to estimate interseismic locking on the subduction fault requires knowing to what degree the slope of the GPS time series represents the interseismic rate (Figure 1). When the noise in the time series is understood, the uncertainty in the slope provides a probability of that being true. To simulate the effect that the distribution of transient offsets has on the slopes of the time series I use a Monte Carlo approach to generate synthetic time series using the observed offsets and interevent times. The spread in the slopes resulting from this procedure is a measure of the uncertainty in the rates.

The offsets in the GeoNet time series used here are due to volcanic sources and slow-slip events; earthquakes and afterslip have been excluded. For a given site and component, the N offsets form an array $A_i(t_i)$ where offset i at time t_i has amplitude A_i, $i = 1, N$. From these a list of N-1 interevent times T_i are derived where $T_i = t_{i+1} - t_i$. Here I am using the observed interevent times for the time dependence, but assuming a Poisson process gives very similar results (few tenths of a mm/yr difference in the estimated slopes). The critical property of the time series that leads to the variability in slopes is that most of the total offset

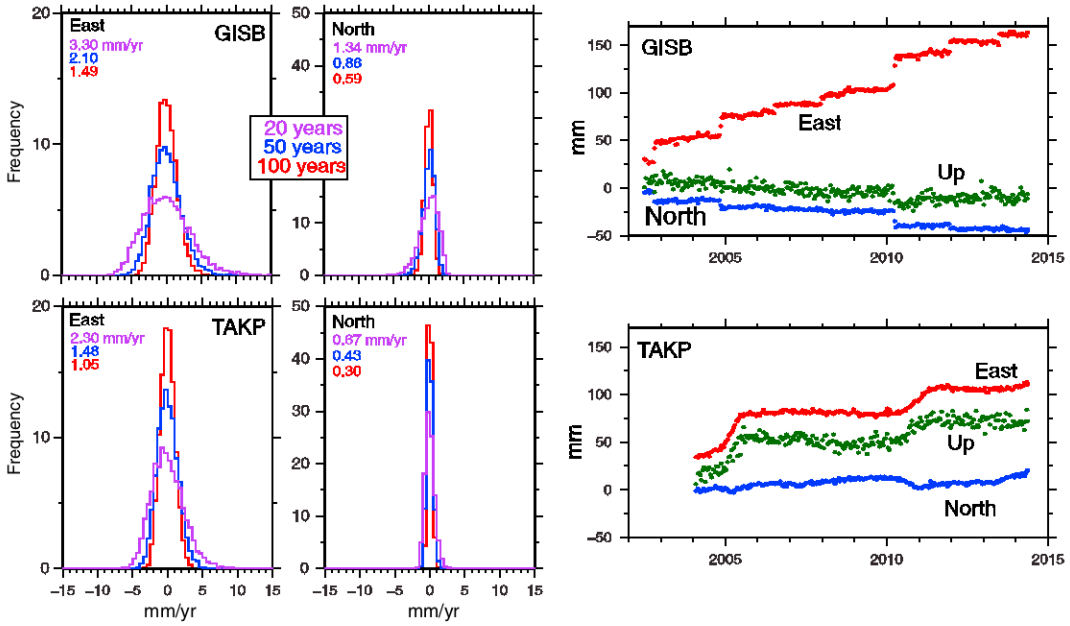

Figure 6. Examples of rate histograms for sites GISB and TAKP showing the frequency of estimated slopes (with means removed) for a Monte Carlo simulation of transient histories. Colors correspond to the duration of the simulated history. Numbers in panels give the standard deviation of the histograms for each time period. The standard deviations of the slopes correspond to rate uncertainties. At the right are time series detrended by their intertransient slopes.

occurs by a few large infrequent events. For example, at GISB, more than half the total offset (~130 mm) from 2005 to 2014 occurs in three events of 33, 22, and 18 mm (Figure 4a).

To simulate a time series X_j of duration T' the algorithm is as follows: (1) Set the time counter t and amplitude a to zero. (2) Select a value T_r at random from the T array. (3) If $t + T_r$ exceeds T', go to step 8. (4) Set $X = a$ from t to $t + T_r$. (5) Select a value A_r at random from the array A and advance a to $a + A_r$. (6) Advance t to $t + T_r$. (7) Go to step 2. (8) Perform linear regression to get slope of X.

The time step used in X is a week. The procedure of generating a synthetic time series in this way is done 5000 times for each site and component, and the standard deviations of their slopes (SDoSs) are used as a measure of the uncertainty in the rate (Figure 6). Two examples of such time series for the east component of GISB (Figure 4c) show how randomizing the events can lead to variable slopes. One simulation has two of the largest (33 mm) events in the 10 year period while the other has none, resulting in a decade difference in velocity of about 6 mm/yr. The simulations were run for the observed duration of each of the time series, then for 10, 20, 50, and 100 years.

For sites where transient offsets are large, the SDoS can be as high as 8 mm/yr for a 10 year observation period (Figure 7a). This level of uncertainty may also apply to the coastal NI2003 survey-mode velocities that have at most ~12 years of data (1991–2003). For many of the cGPS sites with short durations (~6 years) and large SSE, the SDoS for the current time series can be 6 to 8 mm/yr (supporting information).

These SDoSs decrease with time, though slowly (Figures 6 and 7). The SDoS have a strong spatial correlation because the SSE tends to occur along bands, below the coast from 38°S to 41.5°S and farther inland south of 40°S (Figure 4b). Sites in these two regions have the highest SDoS that persist for many decades (Figure 7). It should be noted that these simulations are based on the SSE behavior of the past 14.4 years and do not account for the possibility of larger events or events that may occur on sections of the HSZ that have not yet had them. Fourteen years is not enough time to reveal the full spectrum of SSE behavior, so I expect that these uncertainty estimates might be too low. Below I discuss the possibility of larger, future events.

GPS observations have been made in the North Island for about 20 years, though probably very few sites have this long observation period. The expected SDoS at 20 years (Figure 7b) are still quite high, many exceeding 4 mm/yr in places along the NE coast. The locking models shown earlier indicate that the

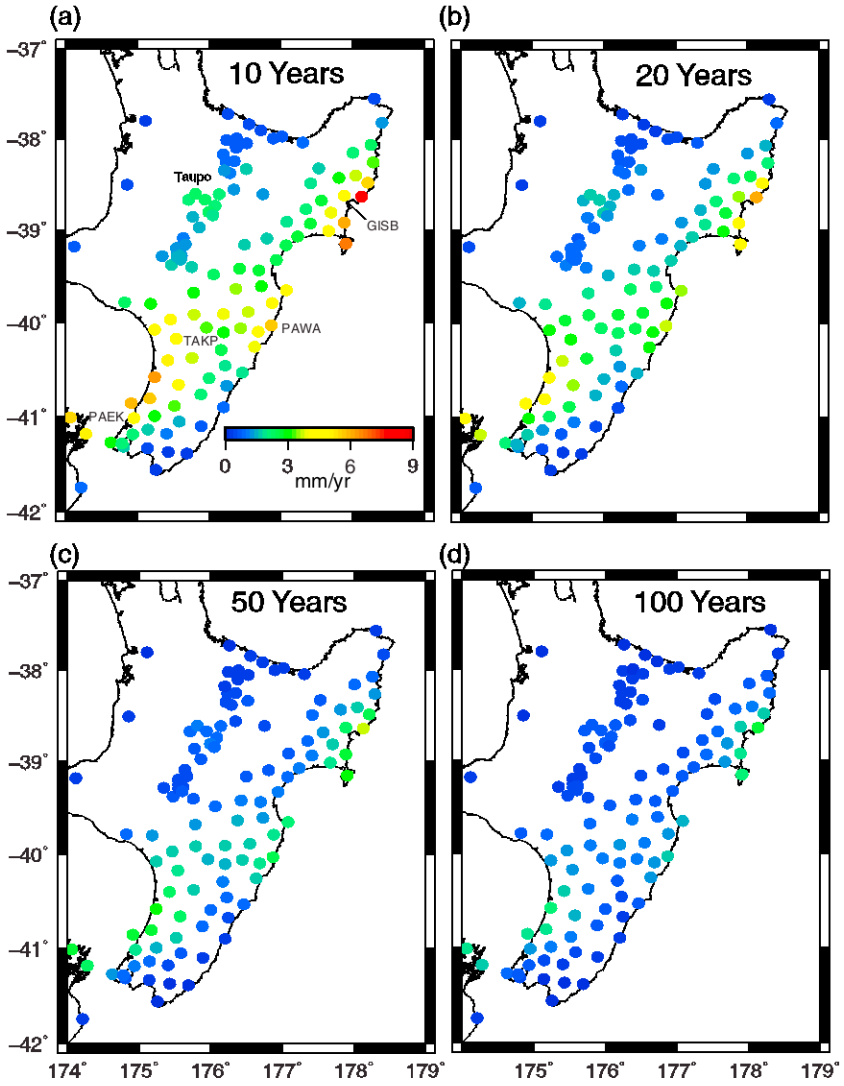

Figure 7. Maps of transient-induced horizontal velocity uncertainties at cGPS sites for different durations of the simulations. Scale bar gives the uncertainty in mm/yr.

westward velocities of sites along the coast due to HSZ locking range from 2 to 5 mm/yr near GISB and 1 to 3 mm/yr farther south near PAWA (Figure 7a). These rates are comparable to the 20 year SDoS arising from slow slip (3.6 mm/yr at GISB and 4.0 mm/yr at PAWA). Hence, the 20 year signal of interseismic locking strain along the north coast may have a low signal-to-noise ratio due to the slow-slip events.

Farther south the sites TAKP (Figure 7a) and PAEK have SSE-induced 20 year SDoS of 2.3 and 2.7 mm/yr, respectively, while their current estimated velocities due to locking range from 3.5 to 4.5 mm/yr and 8 to 10 mm/yr. Accordingly, the signal to noise in the southern HSZ may be higher and provide some better indication of locking than in the north (assuming that the current SSE are typical). The SDoS in the regions of high slow-slip decrease to 2 to 3 mm/yr in the projections at 50 and 100 years (Figures 7c and 7d). In summary, uncertainties in GPS site velocities arising from transient offsets can be several mm/yr, many times larger than a typical uncertainty of ~0.3 mm/yr for a 10 year or more observation period (assuming random walk dominates with a coefficient of 1.0 mm/$\sqrt{\text{yr}}$). In some cases, these uncertainties can be as large or larger than the contemporary signal from subduction locking. To reiterate, if the goal of estimating locking is to compare it to static features of the subduction zone, then these are the velocity uncertainties that should be used.

The Monte Carlo estimates of the SDoS are typically larger than the uncertainties derived by the *Hackl et al.* [2011] method but the correlation is poor (Figure 5b). In a test (supporting information), the two methods

agree when the time series includes offsets forming a zero-mean normal distribution, suggesting that the differences arise from the distribution of observed offsets. *Jiang et al.* [2012] suggested that SSE from Costa Rica could be represented by random walk, but this does not seem to hold for the New Zealand sites.

Using the *Williams* [2003b] approach, I calculate the uncertainties for the New Zealand cGPS time series. For the value of p I use the number of events N with a predicted offset of > 0.1 mm at each site and divided by the total duration of the time series (14.4 years; i.e., $p = N/(14.4 \times 365.25)$); the data variance σ_d^2 is taken from the time series, and the duration T is of the observed time series. The rate uncertainties estimated by Monte Carlo, using the observed distributions of offsets, are generally larger than those estimated by the *Williams* [2003b] method but mostly within a factor of 2 (Figure 5c). (A test with a time series of zero-mean, normally distributed offsets shows agreement between the Monte Carlo and Williams method, see the supporting information.) The Hackl and Williams approaches assume that the noise is stationary, meaning that for long times the expected value is near zero, while the distribution of SSE offsets in New Zealand (Figure 5a) does not meet that criterion. Likely, what is driving the large variations in slopes of the simulated time series are the infrequent, large offset events, generally having the same sense of motion, as demonstrated in Figure 4c.

3.3. Monte Carlo Simulation of SSE and Hikurangi Locking

To explore the impact of the transient velocity perturbations on interseismic locking patterns, we must first take into account that the transient offsets are spatially correlated, and therefore, the site velocities for a given random realization of the velocity field will not be spatially independent. The steps to produce a random velocity field for the cGPS network are similar to those described for the velocity estimates, except in this case all time series are generated together, and the total displacement field for the selected transient event is applied to the network of sites in step 5. After reaching the simulated time period (20 years), all rates are computed and added to the inter-SSE rates. This velocity field represents a random sampling of the SSE as they impact the entire network.

To estimate the locking pattern for each random field, I use the same block model as earlier, the Gaussian locking function and the same starting HSZ locking distribution (a strip of locking between 10 and 25 km depth along the entire margin). I then solve for the block rotations, locking on crustal faults and spatially variable locking on the HSZ. This procedure of generating a velocity field and solving for locking is run over 500 times, and the resulting locking distributions at selected parts of the HSZ are examined (Figure 8).

The tests are designed to assess the sensitivity of long-term locking estimates on the HSZ to GPS velocities that are perturbed by transients. One measure of the variability is in the total moment rate derived from the locking tests (Figure 8 inset). The moment rate of the locking model derived from the 20 year velocities is 3.2×10^{19} N m/yr (Figure 3b) while the moment rates from the test range from 2 to 7×10^{19} N m/yr. This suggests that the slow slip may give rise to a factor of ~2 uncertainty in the long-term locking budget (if the past 14 years are indicative of the SSE pattern).

The resolution for long-term locking at specific points on the subduction zone is evident in histograms of the slip rate deficit (SRD) distributions at the nodes derived from the 500 simulated locking distributions (Figure 8). Where the histograms are broad, resolution for SRD is low because the estimated SRD for a given time period will be highly dependent on the SSE history. In the Gisborne area in the north, the locking resolution is particularly low due to many large transients. The histogram is nearly flat indicating that the slip rate deficit has nearly equal probability of having any of the range of possible values (0 to 45 mm/yr). This effect can be seen in the GISB time series shown in Figure 4a. The 11.5 year average velocity is close to zero (-0.9 mm/yr; east is positive), indicative of little locking, while its intertransient velocity is -11.3 mm/yr, a rapid westward push from the locked plate interface. The difference is due to the transient offsets. At times when transient activity is less, the average velocity will be more negative than it is now, and more locking will be apparent. Downdip from Gisborne the SSE have much less impact—nearly all simulated SRD are below 20 mm/yr, and more than half show no locking.

Below Hawke Bay, where there is no apparent modern locking (Figure 3), the histogram of SRD is fairly flat out to ~35 mm/yr. In ~8 years the coastal site CKID at the south end of the bay (Figures 2 and 4b) has moved ~110 mm to the east in SSEs, an average rate of ~14 mm/yr. If the SSEs were half as energetic, the locking velocity there would be ~ 7 mm/yr which would require considerable locking offshore. Hence, the appearance of the central HSZ being unlocked may be in part a consequence of low resolution there but also

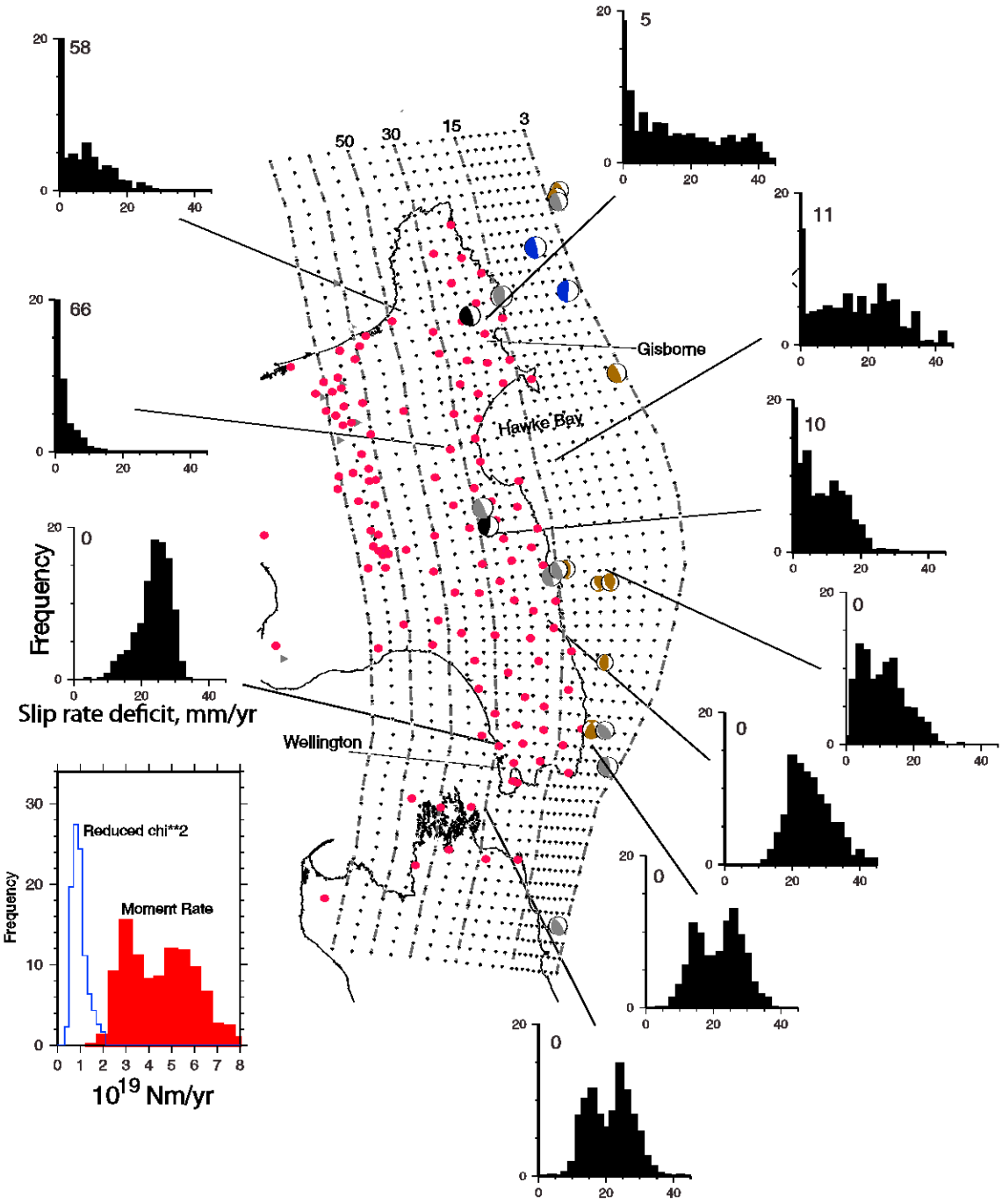

Figure 8. (inset) Histograms of the reduced chi-square misfit (blue) and moment rates (red) for 500 inversions for HSZ locking using 20 year velocities generated from random distributions of transients. Black histograms show the distributions of slip rate deficits (SRDs) resulting from the simulations at selected points on the plate interface. Numbers to right of the frequency axes give the percent of solutions where the SRD went to zero (locking fractions are constrained to be positive in the interseismic period). In these cases, the transient velocities exceeded the locking rate. The broad histograms indicate that a large range of inferred SRD for a 20 year period could result from the effects of transients on the GPS site velocities.

in part the slow-slip keeping pace with the plate convergence over the past 20 years. Some locking there is consistent with evidence for a large earthquake beneath the Hawke Bay [*Cochran et al.*, 2006]. South of Hawke Bay, near the locations of two earthquakes (Figure 7), an area which is weakly locked at present, the histogram indicates that the SRD may be as high as 20 mm/yr. Hence, our knowledge of the interseismic locking in the northern half of HSZ may be quite uncertain.

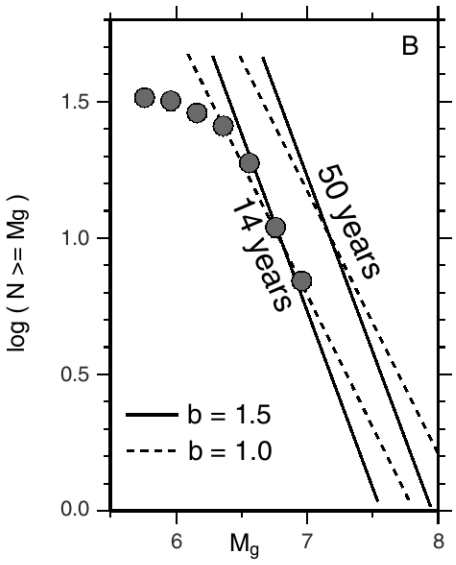

Figure 9. M_g versus log(N) where N is the number of SSE greater than M_g. Dashed lines are for a b value of 1.0, and solid lines are for b value of 1.5. Extrapolating the current distribution of SSE suggests that an $M_g \geq 8.0$ is expected every 50 years (for either b value) if they follow a Gutenberg-Richter distribution.

In the south, the simulations suggest that the range of locking inferred from 20 years of data can span about 2/3 of the possible SRD range (Figure 8). The coastal and offshore regions show moderate to high locking. The coastal sites in this region have only small offsets due to SSE. Locking on the deeper parts of the subduction interface also are not as effected by the SSE because the average SSE velocities in the south are comparable to the velocities due to locking, as noted earlier.

4. Discussion

Locking models for the Hikurangi subduction zone derived from geodetic data have been used along with seismic, structural, and geophysical data to try to understand the controls on locking. The HSZ offers a good location for such studies due to sharp along-strike variations in apparent locking. The simulations described above suggest that some part of these along-strike variations in locking could be ephemeral.

The simulations assume simply that the long-term distribution of SSE is the same as that observed over the past 14.4 years but allow for randomness in the times of occurrence. No allowance was made for any SSE that has not yet occurred. The actual moment frequency distribution of SSE is difficult to ascertain since GPS-detected SSEs generally have covered only about 1 order of magnitude in the moment scale (below 6 are too small to see in GPS and above 7 are rare [*Peng and Gomberg*, 2010]). If the SSE follow a Gutenberg-Richter (G-R)-type frequency distribution, $\log(N) = a - b\,M_g$ where N is the number of events exceeding geodetic moment M_g; most of the moment is in the largest few events, and the resolution of long-term site velocities will be even more difficult to estimate than in the simulation. This problem was described for earthquake occurrence in *McCaffrey* [1997] where simulations of moment rates were made using various earthquake frequency distributions. In general, as the number of small events increased relative to the number of large events (i.e., increasing the b value or steepening of the log(N) versus M_g curve) the impact of the large events on the long-term moment rate lessened. Alternatively, if the b value is lower, the large events dominate and the long-term moment rate estimates are further destabilized. The b value for SSE in New Zealand may be around 1.0 or 1.5 (Figure 9), similar to that observed for earthquakes, although this number is highly uncertain. *Wech et al.* [2010] suggested that the b value for tremor in Cascadia could be near unity. If the SSEs follow G-R and the b value is similar to that for earthquakes, then the SSE moment rates will have similar uncertainties to those of earthquakes [*McCaffrey*, 1997; *Stein and Okal*, 2007]. Our inability to accurately estimate long-term moment rates for subduction zone earthquakes was tragically shown by the 2011 Tohoku-oki earthquake.

If SSE follow Gutenberg-Richter, due to the self-similarity nature of the G-R relationship, larger SSE can be expected because through time the intersection of the log(N) versus M_g curve with the horizontal axis (i.e., $N = 1$) will move toward larger values of M_g. As in the earthquake case, larger M_g events may ultimately be limited by the dimensions of the fault [*Rundle*, 1989] although other factors may impede our ability to observe them [*Meade and Loveless*, 2009]. If $b = 1.0$ or 1.5, then we might expect an SSE at the HSZ in excess of M_g 8 in time frames on the order of 50 years (Figure 9). *Meade and Loveless* [2009] suggested that based on empirical SSE scaling laws, an $M_g = 8$ SSE may slip more slowly than the plate convergence rate and take too long to be recorded as an observable SSE. However, within their bounds an $M_g = 8$ SSE could last 4 years and slip at up to 120 mm/yr, both well within observable windows at the HSZ. If this is the case, then the repeat time of such a large event will ultimately determine how long it will take to obtain a reliable long-term locking picture for the HSZ.

Temporal variations in surface strain rates in the North Island (NI) have been observed for decades, leading to many explanations [see *Webb and Anderson*, 1998]. *Walcott* [1978] noted that in the southern NI extension

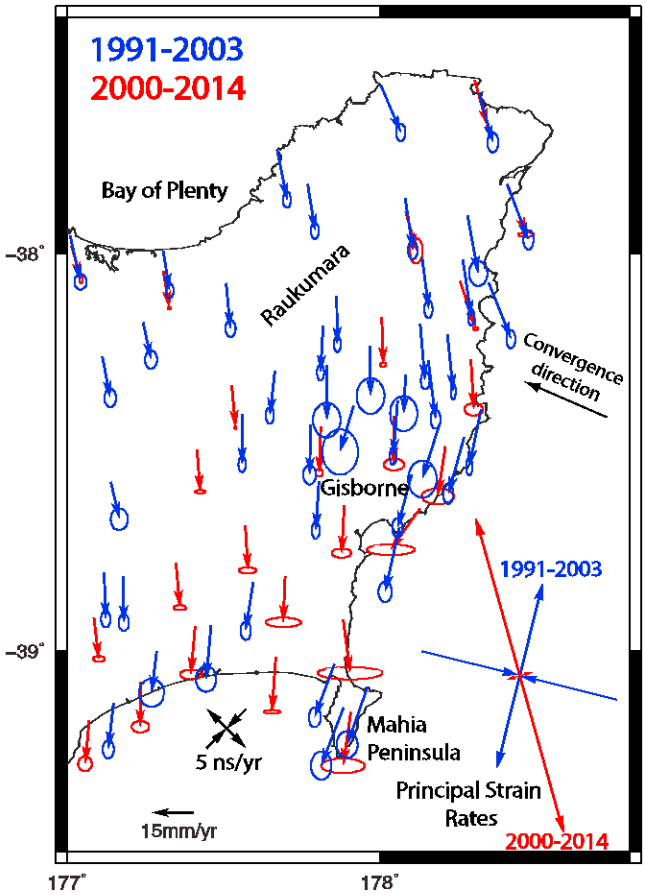

Figure 10. Principal strain rates for the Gisborne-Raukumara region for the time periods 1991–2003 (from B2003 velocity field in blue) and 2000–2014 (from GeoNet cGPS velocity field in red). All vector error ellipses are 70% confidence, and the strain rate uncertainty is about 5 ns/yr (1 ns/yr = 10^{-9}/yr). The strain rate component in the approximate direction of convergence may have reversed sign between the two time periods.

normal to the axial tectonic belt (and subduction zone) occurred up to about 1920, switching over to compression. He suggested that the compression marked the onset of locking on the subduction zone. The simulations described above offer an alternative explanation that the change was part of a long-term SSE cycle and may not be all that unusual. While the southern NI shows less variability than in the north in locking due to SSE in the simulations (Figure 8), it is possible and perhaps likely that the southern NI will experience or has experienced even larger SSEs than have occurred in the past 14 years. If the total slip in the SSE for a given time exceeds the accumulated plate motion (as happens below parts of the NI), the crust may appear to be extending toward the subduction zone. In the south this effect of the SSE has to be larger than in the north because of the significant permanent shortening onshore. *Nicol and Beavan* [2003] estimated that the GPS-derived shortening across the southern NI (at about 40.5°S) comprises 20% permanent strain rate and 80% elastic strain rate from the subduction zone. Hence, for the crust to appear to be in extension, the SSE has to overcome the permanent shortening rate in addition to the elastic rate of loading. However, if the long-term elastic loading rate is lower than in the past 20 years, which is possible, this temporal reversal of strain rates could be a common occurrence.

In the north, at the Raukumara Peninsula, *Arnadottir et al.* [1999] used geodetic data to estimate the strain rates from the 1920s to 1976 and again from 1976 to 1995. They found that for the first time period that the extension direction was approximately normal to the subduction zone and parallel to the HSZ for the second period. While the latter time period may have been consistent with locking on the HSZ, they suggested that the former included deep slip induced by earthquakes. *Meade and Loveless* [2009] suggested that such strain rate fluctuations may arise from larger SSE than already observed, but I suggest that the temporal changes could be caused by variations in the slow-slip history without requiring any larger events (per the simulations). Figure 10 shows the average strain rates estimated from the GPS velocities NI2003 and the cGPS covering two different time spans, 1991–2003 and 2000–2014, respectively, for the region shown within the map. The principal strain rate axes are similar in showing extension in approximately the north-south direction, but the trench-normal component has reversed sign from contraction in the earlier period to slight extension in the latter. One interpretation is that during the period 1991–2003 SSE was less energetic than during 2000–2014. In any case, the apparent paradox of trench-normal extension seen in geodetic data in the Raukumara Peninsula with the history of earthquakes there [*Webb and Anderson*, 1998] can be reconciled by thinking of the strain rates as time dependent, driven by the balance of subduction loading and slow-slip unloading, rather than a steady state feature. The occurrence of earthquakes would suggest that the region is under compression in the interseismic period.

Wallace and Beavan [2010] suggested that the Hikurangi slow-slip events on the HSZ occurred only at the downdip edge of the long-term locking, or near the geodetically inferred transition zone. Their locking model was similar to Figure 3a in which it was assumed that locking was maximum at the deformation front and decreased landward. The better fitting alternative locking model (Figures 3b) that includes some deeper locking reduces this apparent correlation at the HSZ. Globally, this correlation is not particularly robust. In northern Cascadia SSE and tremor occur ~50 km downdip of the locked zone [*Szeliga et al*., 2008], and in Guerrero and central Cascadia (Oregon) the SSE overlap the locked zone [*Graham*, 2013; *Schmalzle et al*., 2014]. The 2012 Costa Rica *M*7.6 earthquake occurred on a patch of the subduction interface where SSE had previously occurred both updip and downdip (T. H. Dixon et al., Earthquake and tsunami forecasts: Relation of slow slip events to subsequent earthquake rupture, submitted to *PNAS*, 2014). The pattern is similar to the relationship between SSE, locking, and earthquakes seen in Figure 3b (dashed line). Along this line, with increasing depth there is SSE, then locking with earthquakes, SSE again, then free slip. As below Costa Rica, slow-slip may occur both updip and downdip of seismic slip.

SSEs near Gisborne have a large offshore slip component (Figure 4b) and thus clearly overlap the locked patch inferred from either the exponential or Gaussian models. Moreover, probable plate interface thrust earthquakes also occur downdip of the slow-slip region in the northern half of the HSZ (Figure 3) indicating that the SSE are not localized at the base of the seismic slip zone. In any case, the temporal complexity of the HSZ and the lack of resolution of offshore locking make it difficult to examine with confidence the relationship between the geodetic transition zone and SSE.

5. Conclusions

Locking at the HSZ over the past 20 years is reexamined. Compared to published locking models, assuming a Gaussian or gridded distribution of locking fits the GPS velocities as well or better and results in deeper locking in the north, with similar depths in the south. The effect of transients on the estimation of long-term GPS site velocities can be profound, larger than the typical formal errors based on power law noise models. For many sites in the North Island, the uncertainties may be larger than 1 to 2 mm/yr for decades to come. In places of little or unknown degrees of locking, SSE may not only decrease the apparent interseismic locking but also severely inhibit our ability to detect it. Accordingly, correlations of the locking patterns with other features of subduction zones should take into account the temporal as well as spatial uncertainties inherent in the geodetic data.

Acknowledgments

The New Zealand GeoNet project and its sponsors EQC, GNS Science, and LINZ, and the late John Beavan provided GPS data used in this study. John Ristau provided the GeoNet focal mechanisms used in Figure 3. Matthias Hackl provided his code for error estimations, and Gina Schmalzle assisted in running it. Bob King and Tom Herring advised on the error analysis. Helpful reviews were provided by Bob King, Jack Loveless, one anonymous reviewer, and the AE. All figures were generated with Generic Mapping Tools [*Wessel and Smith*, 1998]. GeoNet time series data are available at ftp.geonet.org.nz/solutions/regional-filtered, and other data are in the supporting information.

References

Ansell, J. H., and S. C. Bannister (1996), Shallow morphology of the subducted Pacific plate along the Hikurangi margin, New Zealand, *Phys. Earth Planet. Inter.*, *93*, 3–20.

Arnadottir, T., S. Thornley, F. Pollitz, and D. Darby (1999), Spatial and temporal strain rate variations at the northern Hikurangi margin, New Zealand, *J. Geophys. Res.*, *104*, 4931–4944, doi:10.1029/1998JB900109.

Burgette, R. J., R. J. Weldon, and D. A. Schmidt (2009), Interseismic uplift rates for western Oregon and along-strike variation in locking on the Cascadia subduction zone, *J. Geophys. Res.*, *114*, B01408, doi:10.1029/2008JB005679.

Cochran, U., et al. (2006), Paleoecological insights into subduction zone earthquake occurrence, eastern North Island, New Zealand, *Geol. Soc. Am. Bull.*, *118*, 1051–1074, doi:10.1130/B25761.1.

Doser, D. I., and T. H. Webb (2003), Source parameters of large historical (1917–1961) earthquakes, North Island, New Zealand, *Geophys. J. Int.*, *152*, 795–832.

Douglas, A., J. Beavan, L. Wallace, and J. Townend (2005), Slow slip on the northern Hikurangi subduction interface, New Zealand, *Geophys. Res. Letts.*, *32*, L16305, doi:10.1029/2005GL023607.

Eberhart-Phillips, D., and M. Reyners (2012), Imaging the Hikurangi Plate interface region, with improved local-earthquake tomography, *Geophys. J. Int.*, *190*, 1221–1242.

Ekström, G., M. Nettles, and A. M. Dziewonski (2012), The global CMT project 2004–2010: Centroid-moment tensors for 13,017 earthquakes, *Phys. Earth Planet. Inter.*, *200–201*, 1–9, doi:10.1016/j.pepi.2012.04.002.

Goldfinger, C., et al. (2012), Turbidite event history—Methods and implications for Holocene paleoseismicity of the Cascadia subduction zone: U.S. Geological Survey Professional Paper 1661–F, p. 170. [Available at http://pubs.usgs.gov/pp/pp1661f/.]

Graham, S. E. (2013), Earthquake cycle deformation in Mexico and Central America constrained by GPS: Implications for coseismic, post-seismic, and slow slip, PhD thesis, Univ. of Wisconsin, Madison, Wis.

Hackl, M., R. Malservisi, U. Hugentobler, and R. Wonnacott (2011), Estimation of velocity uncertainties from GPS time series: Examples from the analysis of the South African TrigNet network, *J. Geophys. Res.*, *116*, B11404, doi:10.1029/2010JB008142.

Heise, W., T. G. Caldwell, E. A. Bertrand, G. J. Hill, S. L. Bennie, and Y. Ogawa (2013), Changes in electrical resistivity track changes in tectonic plate coupling, *Geophys. Res. Lett.*, *40*, 5029–5033, doi:10.1002/grl.50959.

International Seismological Centre (2011), On-line bulletin, [Available at http://www.isc.ac.uk], Internatl. Seis. Cent., Thatcham, U. K.

Jiang, Y., S. Wdowinski, T. H. Dixon, M. Hackl, M. Protti, and V. Gonzalez (2012), Slow slip events in Costa Rica detected by continuous GPS observations, 2002–2011, *Geochem. Geophys. Geosyst.*, *13*, Q04006, doi:10.1029/2012GC004058.

Loveless, J. P., and B. J. Meade (2010), Geodetic imaging of plate motions, slip rates, and partitioning of deformation in Japan, *J. Geophys. Res.*, *115*, B02410, doi:10.1029/2008JB006248.
McCaffrey, R. (1997), Statistical significance of the seismic coupling coefficient, *Bull. Seismol. Soc. Am.*, *87*, 1069–1073.
McCaffrey, R. (2009), Time-dependent inversion of three-component continuous GPS for steady and transient sources in northern Cascadia, *Geophys. Res. Lett.*, *36*, L07304, doi:10.1029/2008GL036784.
McCaffrey, R. (2013), Steady and transient inter-seismic behavior at the Hikurangi subduction zone, New Zealand: Uncertainties in long-term locking estimates, Eos Trans. AGU, 94, Fall Meet. Suppl., Abstract G44A-01.
McCaffrey, R., A. I. Qamar, R. W. King, R. Wells, G. Khazaradze, C. A. Williams, C. W. Stevens, J. J. Vollick, and P. C. Zwick (2007), Fault locking, block rotation and crustal deformation in the Pacific Northwest, *Geophys. J. Int.*, *169*, 1315–1340.
McCaffrey, R., L. M. Wallace, and J. Beavan (2008), Slow slip and frictional transition at low temperature at the Hikurangi subduction zone, *Nat. Geosci.*, *1*, 316–320.
McCaffrey, R., R. W. King, S. J. Payne, and M. Lancaster (2013), Active tectonics of northwestern US inferred from GPS-derived surface velocities, *J. Geophys. Res. Solid Earth*, *118*, 709–723, doi:10.1029/2012JB009473.
Meade, B. J., and J. P. Loveless (2009), Predicting the geodetic signature of Mw 8 slow slip events, *Geophys. Res. Lett.*, *36*, L01306, doi:10.1029/2008GL036364.
Nicol, A., and J. Beavan (2003), Shortening of an overriding plate and its implications for slip on a subduction thrust, central Hikurangi Margin New Zealand, *Tectonics*, *22*(6), 1070, doi:10.1029/2003TC001521.
Peng, Z., and J. Gomberg (2010), An integrated perspective of the continuum between earthquakes and slow-slip phenomena, *Nat. Geosci.*, *3*, doi:10.1038/NGEO940.
Rundle, J. (1989), Derivation of the complete Gutenberg-Richter magnitude-frequency relation using the principle of scale invariance, *J. Geophys. Res.*, *94*, 12,337–12,342, doi:10.1029/JB094iB09p12337.
Schmalzle, G. M., R. McCaffrey, and K. C. Creager (2014), Central Cascadia subduction zone creep, *Geochem. Geophys. Geosyst.*, *15*, 1515–1532, doi:10.1002/2013GC005172.
Simons, M., et al. (2011), The 2011 Magnitude 9.0 Tohoku-Oki earthquake: Mosaicking the megathrust from seconds to centuries, *Science*, *332*, 1421, doi:10.1126/science.1206731.
Stein, S., and E. A. Okal (2007), Ultralong period seismic study of the December 2004 Indian Ocean earthquake and implications for regional tectonics and the subduction process, *Bull. Seismol. Soc. Am.*, *97*, S279–S295.
Szeliga, W., T. Melbourne, M. Santillan, and M. Miller (2008), GPS constraints on 34 slow slip events within the Cascadia subduction zone, 1997–2005, *J. Geophys. Res.*, *113*, B04404, doi:10.1029/2007JB004948.
Walcott, R. I. (1978), Geodetic strains and large earthquakes in the axial tectonic belt of North Island, New Zealand, *J. Geophys. Res.*, *83*, 4419–4429, doi:10.1029/JB083iB09p04419.
Walcott, R. I. (1984), The kinematics of the plate boundary zone through New Zealand: A comparison of short- and long-term deformations, *Geophys. J. R. Astron. Soc.*, *79*, 613–633.
Wallace, L. M., and J. Beavan (2010), Diverse slow slip behavior at the Hikurangi subduction margin, New Zealand, *J. Geophys. Res.*, *115*, B12402, doi:10.1029/2010JB007717.
Wallace, L. M., J. Beavan, R. McCaffrey, and D. Darby (2004), Subduction zone coupling and tectonic block rotations in the North Island, New Zealand, *J. Geophys. Res.*, *109*, B12406, doi:10.1029/2004JB003241.
Wallace, L. M., P. Barnes, J. Beavan, R. Van Dissen, N. Litchfield, J. Mountjoy, R. Langridge, G. Lamarche, and N. Pondard (2012), The kinematics of a transition from subduction to strike-slip: An example from the central New Zealand plate boundary, *J. Geophys. Res.*, *117*, B02405, doi:10.1029/2011JB008640.
Wang, K., R. Wells, S. Mazzotti, R. Hyndman, and T. Sagiya (2003), A revised dislocation model of interseismic deformation of the Cascadia subduction zone, *J. Geophys. Res.*, *108*(B1), 2026, doi:10.1029/2001JB001227.
Webb, T. H., and H. Anderson (1998), Focal mechanisms of large earthquakes in the North Island of New Zealand: Strain partitioning at an oblique active margin, *Geophys. J. Int.*, *134*, 40–86.
Wech, A. G., K. C. Creager, H. Houston, and J. E. Vidale (2010), An earthquake-like magnitude-frequency distribution of slow slip in northern Cascadia, *Geophys. Res. Lett.*, *37*, L22310, doi:10.1029/2010GL044881.
Wessel, P., and W. H. F. Smith (1998), New, improved version of the Generic Mapping Tools released, *Eos Trans. AGU*, *79*, 579, doi:10.1029/98EO00426.
Williams, S. D. P. (2003a), The effect of coloured noise on the uncertainties of rates estimated from geodetic time series, *J. Geod.*, *76*, 483–494, doi:10.1007/s00190-002-0283-4.
Williams, S. D. P. (2003b), Offsets in Global Positioning System time series, *J. Geophys. Res.*, *108*(B6), 2310, doi:10.1029/2002JB002156.